

<b>Noname manuscript No.</b> (will be inserted by the editor)
--

---

# Testing General Relativity with the Event Horizon Telescope

Dimitrios Psaltis

Received: date / Accepted: date

**Abstract** The Event Horizon Telescope is a millimeter VLBI array that aims to take the first pictures of the black holes in the center of the Milky Way and of the M87 galaxy, with horizon scale resolution. Measurements of the shape and size of the shadows cast by the black holes on the surrounding emission can test the cosmic censorship conjecture and the no-hair theorem and may find evidence for classical effects of the quantum structure of black holes. Observations of coherent structures in the accretion flows may lead to accurate measurements of the spins of the black holes and of other properties of their spacetimes. For Sgr A\*, the black hole in the center of the Milky Way, measurements of the precession of stellar orbits and timing monitoring of orbiting pulsars offer complementary avenues to the gravitational tests with the Event Horizon Telescope.

## Contents

1	Introduction . . . . .	2
2	When Observations and Theory Converge . . . . .	2
3	The Event Horizon Telescope . . . . .	4
4	Why Test General Relativity with the EHT? . . . . .	6
5	Tests with Black-Hole Shadows . . . . .	8
6	Tests with Timing Signatures . . . . .	16
7	Combining Tests with the EHT, Stars, and Pulsars . . . . .	22

---

D. Psaltis  
Department of Astronomy  
The University of Arizona  
933 N Cherry Ave, Tucson, AZ 85711, USA  
E-mail: dpsaltis@email.arizona.edu

## 1 Introduction

The very small size of a black hole makes direct imaging of its environment with horizon-scale resolution a very challenging goal. Taking a picture of the black hole in the center of the Milky Way, which subtends the largest angle in the sky among all known black holes, requires an angular resolution of a few tens of microarcseconds.

At optical wavelengths, achieving microarcsec resolution requires a telescope (or an interferometer) larger than 200 m, which is still unattainable. Recent technological advances at millimeter wavelengths, however, have allowed combining all available millimeter telescopes in the world into a single globe-sized instrument called the Event Horizon Telescope (EHT) that aims to take the first ever images of black holes in the centers of galaxies with horizon scale resolution. These images will allow us to observe directly the interaction of matter and magnetic fields with black hole horizons. Moreover, it will enable us to resolve strong-field general relativistic phenomena that have no weak-field counterparts and perhaps test General Relativity itself.

## 2 When Observations and Theory Converge

Building an instrument with a very high resolution at a given wavelength is not sufficient to take a picture of a black hole. A number of additional conditions need to be satisfied: the Earth's atmosphere (for ground-based instruments), the Galaxy (for the Milky Way black hole), and the accretion flow around the black hole need to be transparent. It turns out that mm-wavelengths satisfy this trifecta of conditions, for reasons that are purely coincidental.

In the case of the central black hole in the Milky Way, Sgr A\*, the transparency of the Galaxy was the first to be studied and verified. Imaging observations in the 1970s at 3.7 cm and 11 cm [1] and, since then, at increasingly shorter radio wavelengths revealed images with sizes that scale with the square of the wavelength  $\lambda$  [2,3,4,5]. These observations were interpreted in terms of detailed models of interstellar scattering [6,7,8] and within the context of additional observations of the scattering screen towards the galactic center [9, 10, 11] as being dominated by the blurring from free electrons in the Galaxy. Extrapolating the expected and observationally verified  $\lambda^2$  dependence of the blurring effect to shorter wavelength led to the conclusion that they will become negligible at mm wavelengths. Later observations at even shorter wavelengths confirmed this by detecting image sizes that deviate from the  $\lambda^2$  law, a result interpreted as caused by resolving the intrinsic size of the accretion flow image [12,13,14,5].

The transparency of the main bulk of the accretion flow was not explored until the mid-1990s. Early attempts to simulate the observational appearance of an accretion flow around a black hole focused on geometrically thin, optically thick accretion disks (these disks are often referred to as Shakura-Sunyaev [15] or Novikov-Thorne disks [16]). Following the work of Refs. [17,

[18], however, it became apparent that, at the low inferred accretion rates of most supermassive black holes in our vicinity, their accretion flows are mostly geometrically thick and optically thin, with the dissipated energy getting primarily advected into the black holes. Soon afterward, the so-called ADAF (advection dominated accretion flows) or, more generally, RIAF (radiatively inefficient accretion flows) models were shown to be consistent with the spectral observations of Sgr A\* [19] as well as of other supermassive black holes, such as the one in center of the M87 galaxy [20]. One of the key predictions of these radiatively inefficient flows (shared also with other models) is the fact that the radio to IR spectra are dominated by self-absorbed synchrotron emission, with the synchrotron photosphere shrinking rapidly with decreasing wavelength.

The parallel efforts that led to the observational evidence for a shrinking size of the image of Sgr A\* and to the theoretical predictions of an increasingly more transparent accretion flow with decreasing wavelength converged at the dawn of the new millennium. Ref. [21] modeled the observed intrinsic image size of Sgr A\* as a function of wavelength in terms of resolving an increasingly more compact self-absorbed emitting region and concluded that, if this trend continues, the size at millimeter wavelengths will be comparable to that of the black-hole horizon. In the context of ADAF models of the accretion flow, Ref. [22] calculated the predicted size of the synchrotron photosphere as a function of wavelength and showed that it was consistent with the then-available observations of Sgr A\* and that the accretion flow would become fully transparent all the way to the horizon at mm-to-IR wavelengths.

The next issue to address, if we were to observe the transparent accretion flow around a black hole with horizon-scale resolution, is what would the signature of the presence of the horizon be. As early as the 1920's, von Laue calculated the cross section of a Schwarzschild black hole to a parallel beam of photons arriving from infinity and found it to have a radius equal to  $\sqrt{27}GM/c^2$ , where  $G$  is the gravitational constant,  $M$  is the black-hole mass, and  $c$  is the speed of light. In 1973, soon after the discovery of the Kerr metric, Bardeen [23] generalized the calculation of the cross section to a spinning black hole. Motivated by Bardeen's work, Ref. [24] calculated horizon-scale images of general geometrically thin disks using very early computational algorithms and hand-drawn (!) visualizations of the results. As computers became more powerful and General Relativistic radiative transfer algorithms became available, so did simulations of the observational appearance of Sgr A\* at horizon scales. Ref. [25] calculated horizon-scale images for Sgr A\* using simple profiles for the electron emissivity in the vicinity of the horizon. In that paper, they also coined the term "black-hole shadow" to refer to the silhouette that a black-hole will cast on the beam of photons. Later on, Ref. [26] calculated horizon-scale images specifically of radiatively inefficient accretion flow models that were shown to agree with all other spectral observations of this source.

The parallel development of theoretical and observational work continued [27, 28, 29, 13] and, in 2008, Doeleman and collaborators made a successful interferometric observation of Sgr A\* at 1.3 mm, using an array comprising

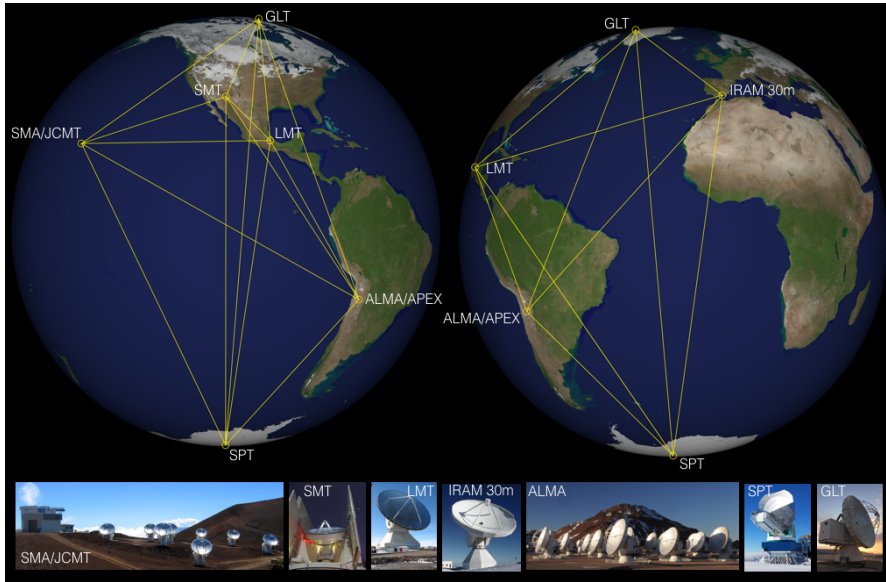


**Fig. 1** The mm telescopes around the world that comprise the Event Horizon Telescope.  
(Credit: D. Marrone/UofA)

only three sites, in Arizona, in California, and in Hawaii [30]. Even though these observations had a very limited baseline coverage to allow imaging of the source, they nevertheless demonstrated that the scale of the image was smaller than  $\simeq 5$  Schwarzschild radii, consistent with the expected size of the black-hole shadow. A similar experiment in 2012 with the black hole in the center of M87 gave comparable results [31]. Both of these observations provided the proof of principle for interferometric imaging of horizon-scale structures in Sgr A\* and M87 at millimeter wavelengths and the impetus for the construction of the Event Horizon Telescope.

### 3 The Event Horizon Telescope

The Event Horizon Telescope (EHT) is a globe-sized array of radio telescopes operating currently at 1.3 mm that aims to capture some of the highest-resolution astronomical images ever made, including the first images of astrophysical black holes with horizon-scale resolution [32]. In its 2018 array configuration, the EHT involved nine stations around the globe: from Hawaii to France and from Greenland to the South Pole.

Early observations with a subset of the array have demonstrated the feasibility of the EHT project. In particular, observations with small subsets of the full array have shown: (i) horizon-scale structures at 1.3 mm for Sgr A\* [30]; (ii) source substructure and variability [33]; (iii) highly polarized emission at horizon scales, indicating the presence of large scale magnetic fields in the

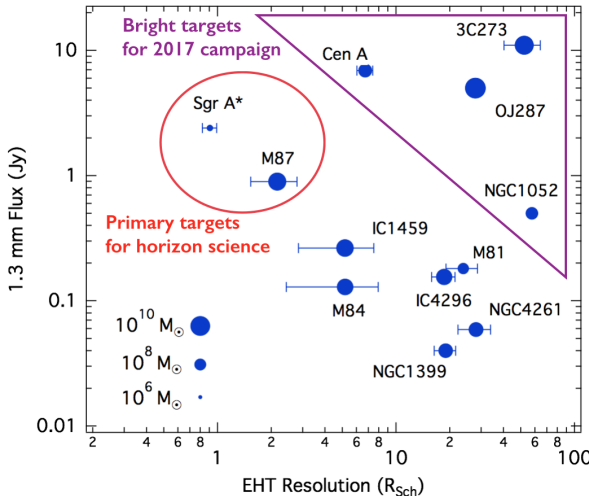


**Fig. 2** Prime targets for observations with the Event Horizon Telescope. The 1.3mm flux and nominal EHT resolution in units of the Schwarzschild radius is shown for a number of known black-hole targets. The two primary targets for horizon-scale science, Sgr A\* and M87, as well as four additional bright targets that were observed during the April 2017 campaign are indicated. The source 3C279, which is also a science target for the array, lies outside the boundaries of this plot.

vicinity of the black hole [34]; and (iv) horizon-scale structure at 1.3 mm for the black hole in the center of M87 [31].

The EHT has since undergone a phase of rapid development and expansion. The first full-array observations were performed in April 2017, with six targets (see Fig. 2). In the case of its two primary targets, Sgr A\* and M87, the EHT is designed to achieve horizon-scale resolution.

In order to exploit the new opportunities that the EHT offers, novel algorithms have been developed to reconstruct images from the interferometric data [35, 36, 37, 38, 39, 40, 41], correct for the blurring effects of interstellar scattering [42, 43, 44, 45], quantify the coherence lengths of magnetic fields near the horizons [46], search for signatures of the black-hole shadows, and perform tests of general relativity [47, 48, 49, 50]. Furthermore, new tools have been implemented to perform Bayesian comparisons of the imaging and timing data to the predictions of semi-analytic models of accretion flows [51], of geometric models of structures [52, 53], and of time-dependent General Relativistic MagnetoHydroDynamic (GRMHD) simulations [54]. Finally, these analysis methods are being validated using large suites of state-of-the-art GRMHD simulations with parameters tuned to match existing observations [55, 56, 57, 58, 59, 60, 46, 61, 62, 63, 64, 65, 66].

The expected images of the shadows cast by the black holes on their surrounding emission, polarimetric maps, and time-variability studies are poised to open novel ways of observing and understanding astrophysical black holes.

Even though a lot will be learned about the interaction of the black holes with the plasma in the accretion flows and in the jets that surrounds their horizons, this review will focus entirely on the prospect of probing and testing General Relativity with EHT observations.

#### 4 Why Test General Relativity with the EHT?

During the last century, many General Relativistic (GR) predictions have been tested in various astrophysical settings. A large number of these tests have been performed within the Solar System, primarily because of the opportunity such tests offer to control systematic uncertainties [67]. More recently, quantitative tests have placed significant constraints on potential modifications of GR at vastly different scales, from the strongest gravitational fields of neutron stars and stellar-mass black holes [68, 69] to the weakest gravitational fields probed by cosmological phenomena [70].

It is often said that GR has passed all these tests with flying colors. This begs the question, then, of why we care to continue testing this theory with black holes, especially in the era of gravitational wave detection from coalescing compact objects with LIGO/VIRGO [71]. There are several motivations for testing GR with the EHT, which I discuss in some detail below; some are primarily empirical and others are mostly theoretical.

First, black-hole spacetimes are qualitatively different than those of other astrophysical objects in terms of testing the underlying theory of gravity. These are the spacetimes in which GR predicts its own demise by forming singularities at their very centers. Moreover, these are the spacetimes that lead to unexpected paradoxes, such as the information paradox [72] and firewalls [73], when one tries to perform calculations with quantum fields in the vicinities of their horizons. Perhaps it is true that all singularities are clothed behind horizons, as the cosmic censorship conjecture postulates. Perhaps the resolution to the information paradox occurs at scales that are too small to be detected observationally. It is quite plausible, however, that the quantum structure of black holes will leave classical, horizon-scale signatures that will be discernible in gravitational tests with black holes [74]. Observations of black holes that resolve horizon scales (either in the electromagnetic spectrum or with gravitational waves) [will allow us to test the cosmic censorship hypothesis](#), measure the properties of their spacetimes, and look for signatures of quantum structures.

Second, the horizon-scale images of the supermassive black holes that will be observed with the EHT probe gravitational fields that are vastly different than those probed in all other GR tests, with or without black holes. Ref. [75] quantified the strength of the gravitational fields probed in different astrophysical systems and by different experiments in terms of the typical magnitude of the gravitational potential and the gravitational curvature in each setting. For a distance  $r$  away from a point mass  $M$ , the gravitational potential and

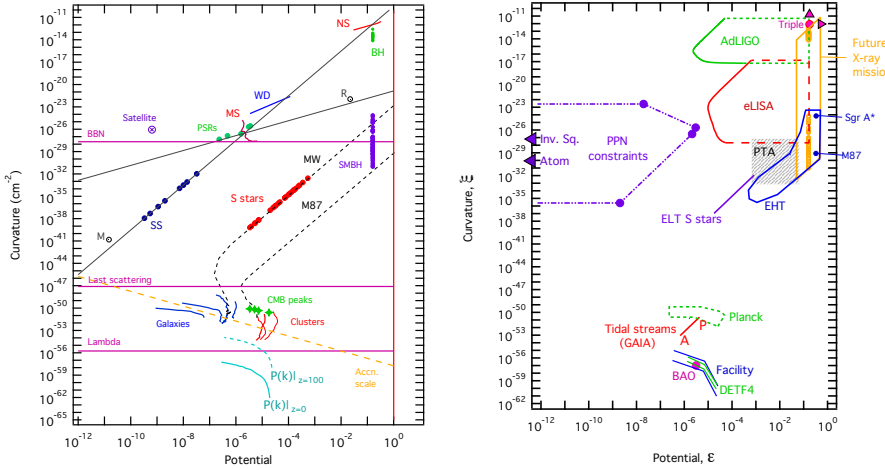


**Fig. 3** The gravitational potential and curvature probed (left) in different astrophysical settings and (right) with different types of observations. The Event Horizon Telescope (EHT) offers the possibility of gravitational tests that are complementary to those of other current and planned experiments, such as those with LIGO/VIRGO, LISA, Pulsar Timing Arrays (PTA), and with optical observations of S-Stars around Sgr A\*. (After Ref. [75].)

curvature are of order

$$\epsilon \equiv \frac{GM}{rc^2} \quad (1)$$

and

$$\xi \equiv \frac{GM}{r^3 c^2}, \quad (2)$$

respectively. (For more precise definitions that are based on invariant quantities and are more broadly applicable, see the discussion in Ref. [75].)

When seen in the parameter space defined by these two quantities (Fig. 3), it becomes clear that the EHT will probe gravitational potentials that are  $\sim 5$  orders of magnitude higher than those of solar system tests and gravitational curvatures that are  $\sim 15 - 20$  orders of magnitude different than those probed by LIGO/VIRGO and by cosmological tests. Even though, in GR, there is no characteristic scale in curvature and, therefore, all astrophysical settings with comparable potentials provide similar constraints, this is not necessarily the case for theories that deviate from GR. As an example, settings with the same potential but different curvatures lead to different gravitational constraints in a large number of theories with screening mechanisms [76]. In the context of tests with compact objects, Ref. [77] showed how black-hole and neutron-star binaries, both of which harbor compact objects of comparable potentials and curvatures, give rise to vastly different constraints on quadratic gravity. Another example that demonstrates the utility of complementary tests at different scales is the recent fifth-force tests with S-stars reported in Ref. [78]. Together with terrestrial (e.g., LIGO/VIRGO, S Star monitoring) and space-based (e.g., LISA) observations, the EHT will provide a complementary and

comprehensive survey of near-horizon gravitational effects with black holes at curvatures that span over 25 orders of magnitude.

Finally, EHT and LIGO/VIRGO tests of GR probe different (albeit highly connected) aspects of the gravitational theory. In GR tests with the EHT, one uses effectively test particles (photons and plasma) to probe the properties of the stationary spacetimes of black holes at very long times after their formation. Because of this, tests with the EHT are actually metric tests and are agnostic with respect to the underlying theory of gravity (as long as it obeys the equivalence principle). In contrast, gravitational waves test the dynamics of the theory during violent merger events and can be used to infer the properties of the stationary metrics only via their dynamics (see the discussion in Ref. [79]). This complementarity is important in tests that involve black holes because a large number of gravitational theories share the exact same black-hole solutions with GR but they differ in the predicted dynamics and gravitational wave signatures [80, 81, 82, 69]. As an example, the shapes and sizes of the shadows of black holes, which the EHT aims to observe, are very sensitive to the quadrupole and higher moments of the stationary black hole spacetimes (see discussion below). For this reason, EHT observations have the potential of testing the no-hair theorem with astrophysical black holes. On the other hand, LIGO/VIRGO observations of gravitational waves measure the time evolution of the quadrupole moments during coalescence but are not currently sensitive enough to measure the moments of the stationary spacetimes during the ring-down phases and test the no-hair theorem [83].

With this motivation in mind, I will now turn into discussing the various gravity tests with EHT observations that have been proposed.

## 5 Tests with Black-Hole Shadows

EHT observations of the two primary targets, Sgr A\* and M87, aim to generate the first images of the shadows the black holes cast on the surrounding emission. Figure 4 shows a compilation of different images at 1.3 mm that are representative of large suites of GRMHD simulations using different algorithms and performed by different researchers. The detailed emission structures are different between images, depending on the way that various simulations treat the initial conditions, the heating of the electrons in the plasma, and the spin and orientation of the black hole with respect to the observer. All images, however, are characterized by a prominent black-hole shadow, which is only partially obscured by intervening plasma orbiting on the equatorial plane.

### 5.1 Properties of Black-Hole Shadows

The outline of a black-hole shadow is determined entirely by the location of the photon orbits and by gravitational lensing. All photons that cross a photon orbit with a momentum vector that point inwards eventually also cross the

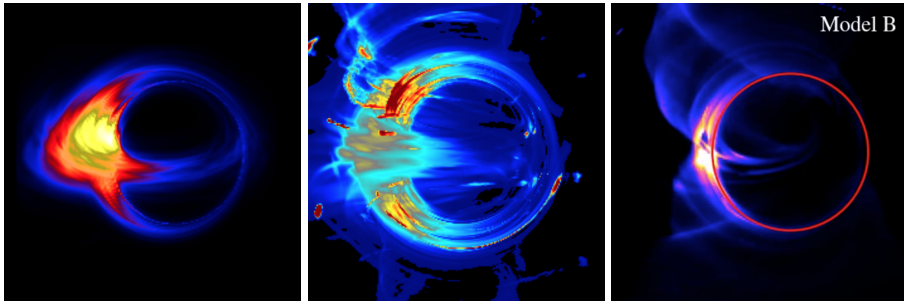


**Fig. 4** Predicted 1.3mm images for Sgr A\* from three different GRMHD simulations [57, 56, 63]. Even though the simulations employ different algorithms and different prescriptions for the sub-grid plasma physics, they all show prominent features at the outline of the black-hole shadow (marked by a red circle in the rightmost panel). The size of the black-hole shadow is  $\sim 10GM/c^2$ .

horizon (in the absence of any additional interaction with plasma) and do not reach distant observers. Because, in an accretion flow, most emission takes place outside the radius of the innermost stable circular orbit (ISCO), which itself is outside the radius of the photon orbit, it follows that most photons that cross the radius of the photon orbit will have inward momenta and will eventually disappear behind the horizon. Therefore, the black hole casts a shadow on the surrounding emission with a size and shape determined by the location of the various photon orbits at different orientations with respect to the black-hole spin axis. The outline of the shadow corresponds to the impact parameters for the trajectories of photons that have barely grazed the corresponding photon orbit. However, its size, as measured by a distant observer, will be larger than the projected radius of the photon orbit, because of gravitational lensing.

For a non-spinning black hole, the Schwarzschild radius of the photon orbit is independent of orientation and equal to

$$r_{\text{ph}} = \frac{3GM}{c^2} . \quad (3)$$

The effect of gravitational lensing is to magnify this to a shadow size of

$$R_{\text{shadow}} = \frac{\sqrt{27}GM}{c^2} . \quad (4)$$

For a spinning black hole, the presence of non-zero multipole mass moments breaks the spherical symmetry of the spacetime. Nevertheless, photon orbits with constant Boyer-Lindquist radii still exist but with distances from the black hole that depend on the orientation of the orbital angular momentum [85]. The existence of closed, spherical photon orbits in a Kerr spacetime is intimately related to the existence of the Carter constant [86]. Because of frame dragging, the radius of a photon orbit depends on the relative orientation of the orbital angular momentum with respect to the black-hole spin.

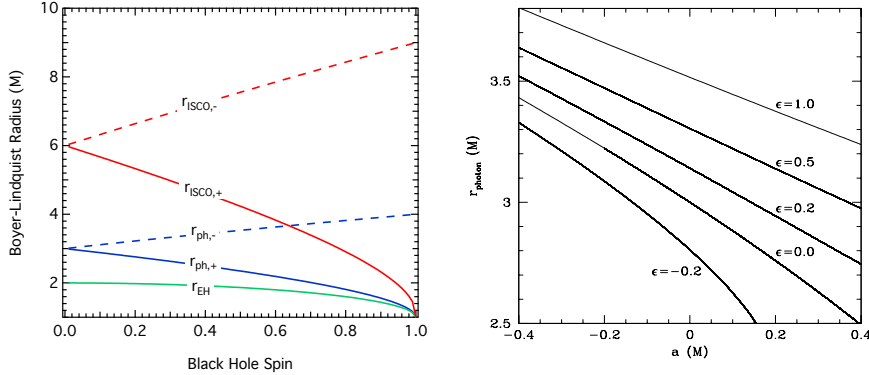


**Fig. 5** (Left) Characteristic radii in the spacetimes of Kerr black holes, as a function of the black-hole spin. Shown are the Boyer-Lindquist radii of the event horizon ( $r_{\text{EH}}$ ), of the prograde and retrograde photon orbits ( $r_{\text{ph},\pm}$ ), and of the prograde and retrograde equatorial ISCO ( $r_{\text{ISCO},\pm}$ ). (After Ref. [23].) (Right) The dependence of the radius of the prograde photon orbit on black-hole spin for spacetimes that violate the no-hair theorem [84]. The parameter  $\epsilon$  measures the deviation of the quadrupole moment of the spacetime from the Kerr value.

For equatorial orbits, the Boyer-Lindquist radii of the prograde (+) and of the retrograde photon orbits (−) are given by [87]

$$r_{\text{ph},\pm} = \frac{2GM}{c^2} \left\{ 1 + \cos \left[ \frac{2}{3} \arccos(\mp|a|) \right] \right\}, \quad (5)$$

where  $0 < |a| \leq 1$  is the specific angular momentum of the black hole per unit mass. Figure 5 shows the Boyer-Lindquist radius of prograde and retrograde photons orbits at different black-hole spins and compares them to the radii of the ISCO and of the event horizon. The multipole mass moments of the spacetime and frame dragging affect also the degree of gravitational lensing that photons experience on their way to a distant observer. The net effect on the outline of the black-hole shadow can still be calculated analytically in the parametric form [23, 88, 89, 90, 49]

$$\begin{aligned} \alpha(r) &= -\frac{[a^2(r+1) + (r-3)r^2] \csc i}{a(r-1)} \left( \frac{GM}{c^2} \right) \\ \beta_{\pm}(r) &= \pm \frac{1}{a(r-1)} \left\{ a^4(r-1)^2 \cos^2 i - [a^2(r+1) + (r-3)r^2]^2 \cot^2 i \right. \\ &\quad \left. - r^3 [(r-3)^2 r - 4a^2] \right\}^{1/2} \left( \frac{GM}{c^2} \right) \end{aligned} \quad (6)$$

Here,  $i$  is the inclination of the observer measured from the spin axis of the black hole, the parameter  $r$  takes values in an interval bounded by  $[r_{\text{ph},-}, r_{\text{ph},+}]$  such that  $\alpha$  and  $\beta$  are real numbers, and  $\alpha$  and  $\beta$  are two orthogonal angular

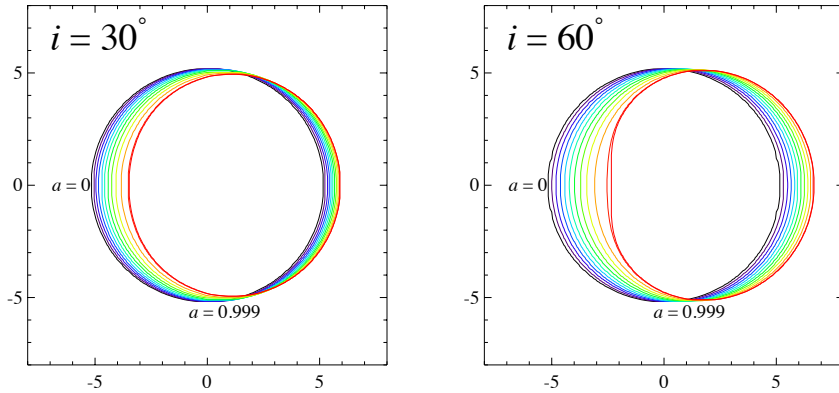


**Fig. 6** The outline of the shadow cast by a Kerr black hole, for different values of the black-hole spin and the inclination of the observer. For all but the highest spins and for all but the highest inclinations, the shadow remains nearly circular, with a radius that depends very weakly on spin or inclination.

coordinates on the image plane of a distant observer with  $\alpha$  perpendicular to the spin axis of the black hole.

Figure 6 shows the outline of a black-hole shadow for different spins and different inclinations of the observer. There are a number of immediate results that can be seen from this picture:

(i) *The size of the shadow of a Kerr black hole depends extremely weakly on spin and inclination.* We can calculate the half opening angle (“radius”) of the shadow on the spin equator for  $i = \pi/2$  as

$$\begin{aligned} R_{\text{shadow,eq}} &= \frac{1}{2} [\alpha(r_{\text{ph},+}) - \alpha(r_{\text{ph},-})] \\ &\simeq \frac{\sqrt{27}GM}{c^2} \left(1 - \frac{a^2}{18}\right) + \mathcal{O}(a^4). \end{aligned} \quad (7)$$

Equation (7) as well as a more systematic study of the size of the shadow averaged over different directions with respect to its center [47] show that, for all black-hole spins and observer inclinations (see Fig. 7),

$$\langle R_{\text{shadow}} \rangle \simeq \frac{5GM}{c^2} \pm 4\%. \quad (8)$$

(ii) *The center of the black-hole shadow does not coincide with the projected position of the origin of the spacetime.* We can calculate the position of the center of the black-hole shadow for  $i = \pi/2$  as

$$D = \frac{1}{2} [\alpha(r_{\text{ph},+}) + \alpha(r_{\text{ph},-})] \simeq -2a. \quad (9)$$

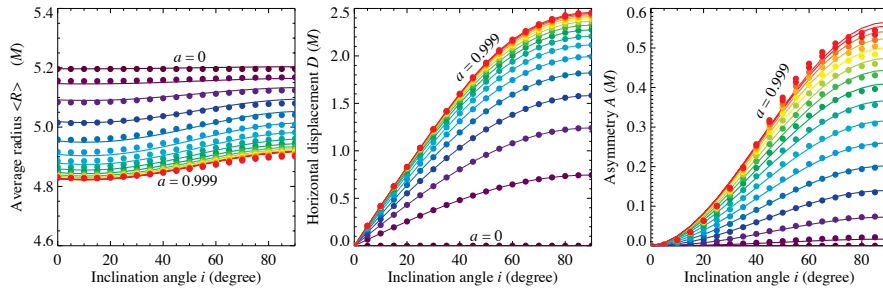


**Fig. 7** The average radius, horizontal displacement, and asymmetry of the shadow of a Kerr black hole, for different black-hole spins and observer inclinations [91].

A more systematic study of the size of the shadow averaged over different directions with respect to its center [90, 47] show that, for all black-hole spins and observer inclinations (see Fig. 7),

$$D \simeq -2a \sin i . \quad (10)$$

(iii) *The black-hole shadow is nearly circular for all but the highest values of its spin.* Different definitions and approximate expressions exist in the literature for the degree of asymmetry of the shadow [90, 47, 91, 92]. They all show a very small degree of asymmetry that, even for the most rapidly spinning black holes, is  $\leq 5\%$  (see Fig. 7).

It is surprising that, even though all properties of the Kerr spacetime (e.g., the horizon, the location of the ISCO, the location of the photon orbit) depend very strongly on the spin of the black hole (see Fig. 5), the shape and size of its shadow remains remarkably constant. This has been understood as the result of the near cancellation of the effects of the spacetime quadrupole and of frame dragging [47]. The quadrupole moment of the spacetime breaks the spherical symmetry of the problem and would have caused the black-hole shadow to appear highly elliptical. However, photons that propagate in the same direction as the black-hole spin experience the opposite effect of frame dragging along their trajectories compared to photons that propagate in the opposite direction. When the spacetime spin  $a$  and quadrupole  $q$  obey the Kerr relation,  $q = -a^2$ , these two effects nearly cancel each other, causing the black-hole shadow do be nearly circular and displaced.

## 5.2 Proposed Tests

The properties of black-hole shadows that are summarized in Fig. 7 have led to a number of proposed tests of gravity:

*Cosmic Censorship Tests.*— Ref. [93] proposed a test of the cosmic censorship hypothesis based on using observations of black-hole shadows to differentiate between Kerr metrics that are surrounded by horizons (i.e., for  $a \leq 1$ ) and

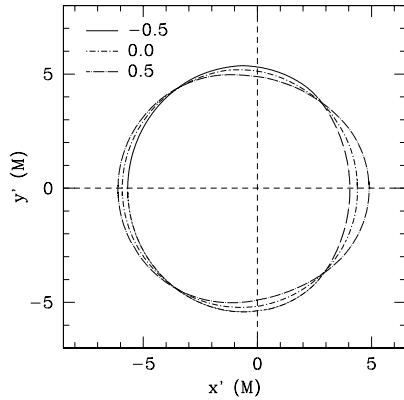


**Fig. 8** Asymmetric black-hole shadows from quasi-Kerr spacetimes that violate the no-hair theorem [47].

those that are not ( $a > 1$ ). This test can be extended to spacetimes of naked singularities that are not described by the Kerr solution (see, e.g., Ref. [94]). The conclusion of these studies is that the detection of a black-hole shadow is *not* a proof of the presence of an event horizon; naked singularities may also show shadows, depending on their parameters. When they do not show shadows, the resulting images are characterized by brightness profiles that are very centrally peaked. When they do show shadows, their shapes are often very unusual and their sizes can be significantly different from those of Kerr black holes. If EHT observations provide conclusive evidence for the presence of shadows in the images of the primary targets, then cosmic censorship tests can be performed in parallel with the null-hypothesis, no-hair theorem, and metric tests described below, all of which also rely on measuring the shapes and sizes of the shadows.

*Null Hypothesis Tests.*— Ref. [96] proposed a null hypothesis test of the Kerr spacetime that is based on the fact that the shadows of Kerr black holes have radii (in gravitational units) that span only a very narrow range. The apparent radius of a black hole shadow depends primarily on the ratio of the mass  $M$  to the distance  $D_{\text{BH}}$  of the black hole. For Sgr A\*, monitoring of the orbits of stars in the vicinity of the black hole have constrained this ratio, which corresponds to the angular size in the sky of one gravitational radius located at the distance of Sgr A\*, to

$$\frac{GM}{D_{\text{BH}}c^2} = 5.09 \pm 0.17 \mu\text{as}. \quad (11)$$

Combining this measurement with the expected range of sizes of the shadow for different black-hole spins and observer inclinations leads to a prediction for

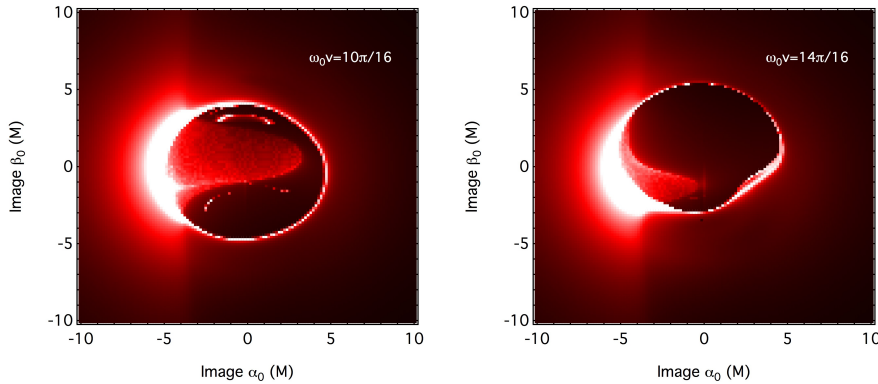


**Fig. 9** Two snapshots of the time-dependent black-hole shadow calculated in Ref. [95] for a spacetime that is characterized by quantum fluctuations at horizon scales.

the half angular size of the shadow of Sgr A\* in the sky of [97]

$$\delta\theta_{\text{SgrA}*} = 25.5 \pm 0.9 \mu\text{as} . \quad (12)$$

This prediction has no free parameters. If EHT measurements of the size of the black-hole shadow in Sgr A\* find it inconsistent with this prediction, then the null hypothesis (i.e., that Sgr A\* is described by the Kerr metric) will be falsified.

*Tests of the No-Hair Theorem and of non-Kerr metrics.*— Ref. [47] proposed a test of the no-hair theorem based on the fact that the shadow of a black hole is nearly circular only if its spacetime obeys the particular relation between the quadrupole moment and its spin that is dictated by the no-hair theorem, i.e., if  $q = -a^2$ . If we allow for violation of the no-hair theorem, i.e., allow for the quadrupole moment of the spacetime to take arbitrary values, then the black-hole shadow becomes asymmetric and its size can take significantly larger or smaller values than what is given by equation (8). The outlines of black-hole shadows have since been calculated for a large number of metric that are either parametric extensions of the Kerr metric or solutions to non-GR field equations [98, 99, 100, 101, 102, 103, 104, 105, 106, 107, 108, 109, 110, 111, 112, 113, 114, 115, 116, 117, 118] (see, e.g., Fig. 8). The shadows for these spacetimes become asymmetric even at small values of the spin because the effect of the spacetime quadrupole and of frame dragging do not nearly cancel each other. In other words, measuring the size and shape of the black hole shadow and comparing the measurements to the values predicted for the Kerr metric leads to a direct test of the no-hair theorem.

*Tests of Quantum Structure.*— All the tests of black-hole metrics discussed above search for deviations in the structures of stationary spacetimes. It is plausible, however, that the spacetimes of black holes appear to have classical dynamics because of quantum fluctuations at horizon scales [74]. Ref. [95]

explored the impact of such fluctuations on the properties of the shadows cast by black holes. They found that horizon-scale fluctuations of the spacetime with even small amplitudes lead to order unity fluctuations of the shape and size of the shadow (see Fig. 9). The characteristic timescale of fluctuations would be  $\sim 1$  hr for Sgr A\* and  $\sim 60$  d for M87. Given that it takes several hours for the EHT to generate a single image, it will require non-imaging techniques to disentangle such signatures from the raw EHT data of Sgr A\*. On the other hand, such fluctuations will be readily visible in the individual snapshots of M87 taken months or years apart.

### 5.3 Implementation and Challenges

The shape and size of the shadow of a black hole depends only on the black-hole spacetime. As a result, *tests of gravity that involve the properties of black-hole shadows are free from any astrophysical complications*. The presence of an accretion flow around the black hole is necessary as a source of radiation on which the black hole can cast its shadow. However, the intricacies of the thermodynamics of its plasma, the structure of its turbulent magnetic fields, and its emission properties, i.e., all of the issues that make predictions in accretion physics difficult, do not affect the shadows of the black holes.

The main complication introduced by the accretion flow is the fact that it may be obscuring, partially or fully, the shadow. This would have been especially important had the accretion flow been optically thick [24, 119], which is not the case for the primary targets Sgr A\* and M87 (see discussion in §2). However, even for the radiatively inefficient flows of those black holes, the left-right brightness asymmetry of the accretion flow (with respect to its angular momentum axis) caused by relativistic Doppler effects (see Figure 4) and obscuration by the plasma intervening between the observer and the event horizon (see, e.g., Ref. [120, 63, 121]) require special care in the measurement of the shadow shape and size.

In principle, the properties of the black-hole shadow and, hence, of the underlying spacetime, can be inferred indirectly by fitting models of the accretion flow in different spacetimes to EHT observations [48]. This approach, however, depends very strongly on the predictive power of accretion models and is, therefore, susceptible to biases. To overcome this limitation, two alternative approaches have been suggested that focus entirely on measuring characteristics of the shadow and not of the accretion flow.

Refs. [47, 122] proposed measuring the shape and size of the bright ring of light that surrounds the black-hole shadow. This ring of light is the result of photon paths that graze the various photon orbits and circle the black hole a very large number of times before emerging towards a distant observer. The total emissivity integrated along such photon paths becomes very large and causes the narrow but bright ring of light surrounding the shadow (see discussion in Ref. [47]). In principle, the narrow width of the bright ring allows for a precise measurement of its shape and size [122]. The applicability of this

approach, however, might be limited by the fact that the ring of light will be hard to distinguish from the bright accretion flow image, especially towards the side that is Doppler boosted towards the observer and, hence, very bright.

A second characteristic of a black-hole shadow is the very abrupt change in the image brightness across it. In other words, the outline of the shadow of a black hole is the locus of points in the image with the highest gradient in brightness. Ref. [49] proposed employing edge detection algorithms to identify the locations of points on an image with the highest gradients and then applying a pattern matching Hough/Radon transform in order to measure the properties of the shadow. The benefits of this approach is that it filters out all the flux that arises from the accretion flow and, therefore, its associated complexities. However, for the case of Sgr A\*, this approach relies on an accurate mitigation algorithm for the effects of interstellar scattering, which blurs the image and smooths the sharp edge at the black-hole shadow.

The litmus test for any investigation on black-hole spacetimes that relies on black-hole shadows is the verification that the same shadow shapes and sizes are measured in repeated observations separated by many dynamical timescales (hours for Sgr A\* and months for M87). Furthermore, because gravitational effects are achromatic whereas plasma effects are not, the measurements of shadow shapes and sizes will need to be consistent among observations at different wavelengths and at different polarizations. The EHT will be observing its targets over multiple days during an observing season, over multiple years, with polarization information, and at two wavelengths (at least), i.e., 1.3 mm and 0.86 mm, offering many opportunities to verify any measurements and to perform such consistency tests.

## 6 Tests with Timing Signatures

The flux of radiation that emerges from accreting black holes has been observed to be highly variable at all mass scales, from stellar-mass black holes [123] to supermassive black-holes, such as Sgr A\* [124, 125, 126]. This is expected given the turbulent nature of the accretion flow and the caustic properties of lensing in black-hole spacetimes [127, 128]. For the case of Sgr A\*, observations in the infrared and in the millimeter have shown that the variability is characterized by a broad band, red noise spectrum with a potential turn-over at timescales longer than a few hours [129, 130]. For M87, a similar turn-over occurs at tens of days [131].

In the case of stellar-mass black holes, observations can track black-hole variability over millions of dynamical timescales, which are as short as a few milliseconds. The surprising results of such studies has been the discovery of quasi-periodic oscillations, primarily in the X-ray flux, with very high quality factors [123] and regular and reproducible properties [132]. The origin of these oscillations is not understood but their high coherences suggest that they are the observational manifestations of linear [133, 134] or resonant [135] oscillatory modes in the accretion flows. This opens the possibility that the EHT

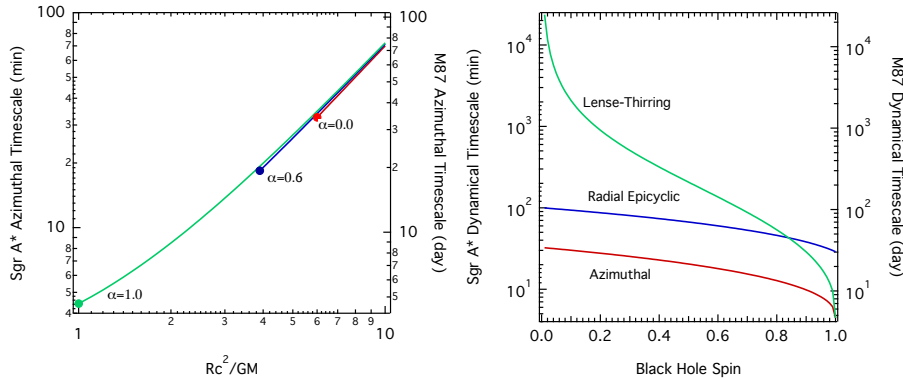


**Fig. 10** (Left) The dynamical timescale for azimuthal (orbital) motions of test particles around a black hole, as a function of the location of the orbit, for three different values of the black-hole spin. The filled circles mark the location of the ISCO. (Right) The characteristic dynamical timescales for the azimuthal motion of a test particle at the ISCO, for the radial epicyclic motion at the location of the peak radial frequency, and for the Lense-Thirring precession at the location of the ISCO, as a function of the black-hole spin. The latter two timescales are expected to be comparable to the periods of  $g$ - and  $c$ -modes excited in the inner accretion flows. In both panels, the left axes show the timescales in minutes for the mass of Sgr A\* and the right axes show the timescales in days for the mass of M87.

images will show compact coherent structures (e.g., the nodes of the oscillatory modes that will appear as “hot spots”) with fluxes or relative positions on the images that oscillate in a quasi-periodic fashion for tens of cycles. The expected frequencies of oscillations trace closely dynamical frequencies in the black-hole spacetimes, offering the possibility for additional gravity tests with EHT data.

### 6.1 Properties of Timing Signatures

We can define three dynamical frequencies at any given location in the space-time of a spinning black hole. For a test particle at a Boyer-Lindquist radius  $r$ , the azimuthal frequency, which describes the frequency of circular orbital motion as measured by an observer at infinity, is given by [23]

$$\Omega_\phi = \left( \frac{GM}{c^3} \right)^{-1} \frac{1}{(rc^2/GM)^{3/2} \pm a}, \quad (13)$$

where, hereafter, the  $\pm$  sign corresponds to prograde and retrograde orbits. The corresponding dynamical timescale for the two primary targets becomes

$$\begin{aligned} \tau_\phi &\equiv \frac{2\pi}{\Omega_\phi} = 2.2 \left( \frac{M_{\text{SgrA*}}}{4.3 \times 10^6 M_\odot} \right) \left[ \left( \frac{rc^2}{GM_{\text{SgrA*}}} \right)^{3/2} \pm a \right] \text{ min} \\ &= 2.3 \left( \frac{M_{\text{M87}}}{6.5 \times 10^9 M_\odot} \right) \left[ \left( \frac{rc^2}{GM_{\text{M87}}} \right)^{3/2} \pm a \right] \text{ d}. \end{aligned} \quad (14)$$

(Note that, because of the mass difference between Sgr A\* and M87, one minute for Sgr A\* corresponds to one day for M87).

The azimuthal dynamical timescale is an increasing function of radius (see also Fig. 10). Stable circular orbits exist only outside the ISCO, the radius of which is given by [23]

$$r_{\text{ISCO}} = 3 + Z_2 \mp [(1 - Z_1)(3 + Z_1 + 2Z_2)]^{1/2}, \quad (15)$$

where

$$Z_1 = 1 + (1 - a^2)^{1/3} \left[ (1 + a)^{1/3} + (1 - a)^{1/3} \right] \quad (16)$$

$$Z_2 = (3a^2 + Z_1^2)^{1/2}. \quad (17)$$

As a result, the shortest azimuthal dynamical timescale that corresponds to stable motions is equal to  $\tau_\phi(r_{\text{ISCO}})$  and depends only on the black-hole spin. This is shown in the right panel of Figure 10. For Sgr A\*, it varies from  $\sim 33$  min for zero spin to  $\sim 4.4$  min for maximum spin and, for M87, it varies between  $\sim 30 - 4$  days. This is the fastest dynamical timescale in an accretion flow and no significant variability is expected to occur at faster timescales [136]. Indeed, this expectation has been verified in the case of stellar-mass black holes [137, 123].

The radial epicyclic frequency, which describes the frequency of the radial oscillations of a test particle in orbit, as measured by an observer at infinity, is given by [138]

$$\kappa = \Omega_\phi \left[ 1 - 6 \frac{GM}{rc^2} - 3a^2 \left( \frac{GM}{rc^2} \right)^2 \pm 8a \left( \frac{GM}{rc^2} \right)^{3/2} \right]^{1/2}. \quad (18)$$

For radii close to the black hole, the radial epicyclic frequency becomes increasingly smaller than the azimuthal frequency. In fact, the radial epicyclic frequency has a maximum at some characteristic radius (equal to  $8GM/c^2$  for a non-spinning black hole) and, by definition, vanishes at the location of the ISCO. Linear gravity modes (or g-modes) can be excited and trapped with frequencies comparable to the maximum of the radial epicyclic frequency (see, e.g., Ref [139]). For a non-spinning black hole, the characteristic dynamical timescale that corresponds to the maximum radial epicyclic frequency (and, hence, to the fundamental g-mode) is

$$\begin{aligned} \tau_r &\equiv \frac{2\pi}{\kappa} = 100 \left( \frac{M_{\text{SgrA*}}}{4.3 \times 10^6 M_\odot} \right) \text{ min} \\ &= 105 \left( \frac{M_{\text{M87}}}{6.5 \times 10^9 M_\odot} \right) \text{ d}. \end{aligned} \quad (19)$$

Figure 10 shows that the radial timescale decreases with increasing spin of the black hole and reduces to  $\sim 30$  min for Sgr A\* and to  $\sim 30$  d for M87.

Finally, the vertical epicyclic frequency, which describes the frequency of vertical oscillations of a test particle in orbit, as measured by an observer at infinity, is given by [140]

$$\Omega_{\perp} = \Omega_{\phi} \left[ 1 - 4a \left( \frac{GM}{rc^2} \right)^{3/2} + 3\alpha^2 \left( \frac{GM}{rc^2} \right)^2 \right]^{1/2}. \quad (20)$$

Linear corrugation modes (or c-modes) can be excited at the innermost regions of the accretion flow, with frequencies comparable to the Lense-Thirring frequency (see, e.g., Ref. [141])

$$\Omega_{LT} \equiv \Omega_{\phi} - \Omega_{\perp} \quad (21)$$

that measures the precession frequency of the orbital plane of the test particle. For a slowly spinning black hole, the characteristic dynamical timescale that corresponds to the Lense-Thirring frequency (and hence to the fundamental c-mode) at the ISCO is

$$\begin{aligned} \tau_{LT} &\equiv \frac{2\pi}{\Omega_{LT}} = 2400 \left( \frac{a}{0.1} \right)^{-1} \left( \frac{M_{SgrA*}}{4.3 \times 10^6 M_{\odot}} \right) \text{ min} \\ &= 2520 \left( \frac{a}{0.1} \right)^{-1} \left( \frac{M_{M87}}{6.5 \times 10^9 M_{\odot}} \right) \text{ d}. \end{aligned} \quad (22)$$

Figure 10 shows that the Lense-Thirring timescale decreases rapidly with increasing spin of the black hole and actually becomes shorter than the radial timescale for spins larger than  $\sim 0.85$ .

The timescales shown in Figure 10 are comparable to the expected periods of linear modes in the accretion flows that are trapped in the frequency cavities dictated by the Kerr spacetime, with small corrections due to hydrodynamic effects. However, it is plausible that same modes at different locations and with different frequencies may become resonant, reaching large observable amplitudes [135]. This appears to be the case for some (but not all) pairs of simultaneous quasi-periodic oscillations observed from stellar-mass black holes with frequencies in 3:2 ratios (or similar ratios of small integers).

It is important to emphasize here that orbiting coherent structures that lead to large-amplitude, quasi-periodic oscillations in the images and brightness of accreting black holes have not been seen in any of the numerical simulations discussed earlier. However, this is most likely a shortcoming of the simulations. Nature somehow manages to generate quasi-periodic oscillations in stellar-mass black holes with structures that last for tens of cycles and modulate large fractions (more than 10%) of the total accretion luminosity.

## 6.2 Proposed Tests

Figure 10 shows that the fundamental periods of different accretion disk modes have different dependencies on black-hole spin. As a result, identifying at least

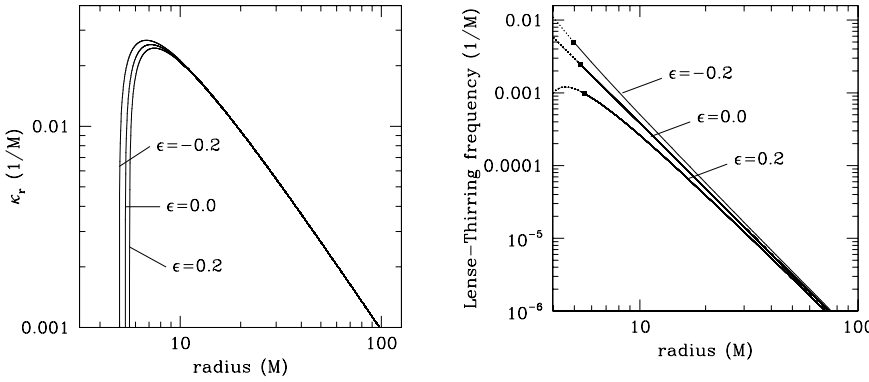


**Fig. 11** The (*Left*) radial epicyclic and the (*Right*) Lense-Thirring frequency as a function of radius in the spacetime of an object that deviates from the Kerr metric. The parameter  $\epsilon$  measures the degree to which the spacetime violates the no-hair theorem. (After Ref. [147].)

two of these modes and measuring their frequencies leads to a measurement of the black-hole spin [142, 143, 144, 145, 146]. Similar to the case of helioseismology, each fundamental oscillatory mode is accompanied by a larger spectrum of high-order modes, allowing for the mode identification to be verified, if such a spectrum can be detected..

Ref. [147] proposed that identifying three modes around a black-hole of known mass and measuring their frequencies can lead to a test of the Kerr metric (see also [148]). This test can be cast, in principle, as a null-hypothesis test. In other words, two of the frequencies can be used to measure the black-hole spin and this information can then be used to predict the third frequency, with no free parameters, and compare it to the observed value. Alternatively, the same approach can be formulated as a test of the no-hair theorem. To this end, Ref. [147] calculated the characteristic dynamical frequencies in a quasi-Kerr spacetime with a quadrupole moment that deviates by an amount  $\epsilon = q + a^2$  from the Kerr value (see Fig. 11). They found that the azimuthal ( $\Omega_\phi$ ) and the radial epicyclic frequencies ( $\kappa$ ) show a very similar dependence on the deviation parameter and can be used primarily to measure the black-hole spin. On the other hand, the Lense-Thirring frequency, which corresponds to the frequency of the c-mode shows an orthogonal dependence on the deviation parameter and is optimal in measuring its value and verifying how close to zero it is.

### 6.3 Implementation and Challenges

The EHT typically observes its two primary targets for a few hours during a small number of nearly consecutive days and repeats the observations 12

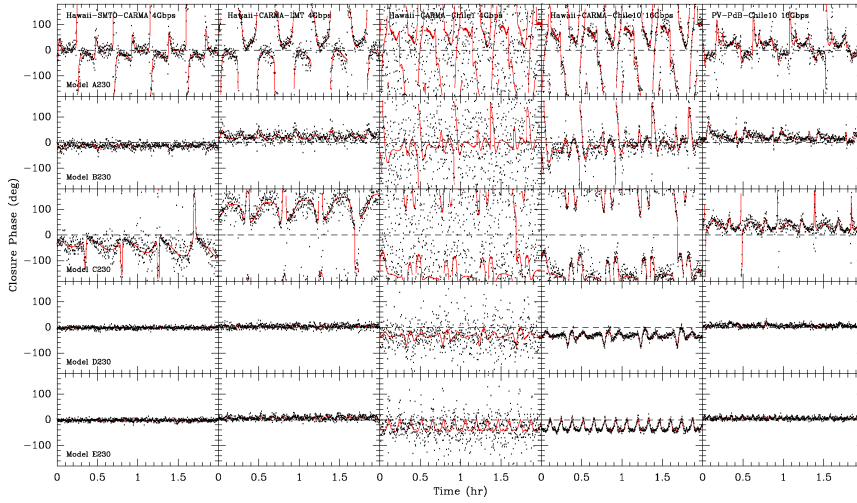


**Fig. 12** Closure phases at different triangles of baselines (*columns*) and for different models (*rows*) of compact emission regions in orbit around Sgr A\*. The detection of correlated, quasi-periodic oscillations in such closure phases with the Event Horizon Telescope may lead to measurements of the frequencies of oscillatory modes in the accretion flows and the properties of their spacetimes. (After Ref. [149].)

months later, when the weather conditions and the elevation of the targets are optimal at all telescope locations. Because the characteristic timescales of variability in M87 for, e.g., the azimuthal and radial modes range between 4 and 100 days (see Figure 10), the cadence of observations is not optimal for sampling several cycles of the expected variability.

The situation for Sgr A\* is exactly the opposite. The corresponding characteristic variability timescales range from 4 to 100 minutes (or 0.07 to 1.7 hours), which is nicely sampled by the cadence of observations. However, these timescales are substantial shorter than the several hours it takes for the Earth to rotate and the baselines to cover a substantial fraction of the interferometric space to generate an image. As a result, tests of gravity with timing signatures in Sgr A\* need to employ non-imaging techniques.

Ref. [149] proposed using the time variability of closure phases along different baseline triangles to search for such timing signatures (see also [150]). A closure phase is the sum of the complex visibility phases along three baselines that form a closed triangle. Closure phases can be measured accurately with a fast cadence and are independent of atmospheric delays and telescope gains, both of which are hard to calibrate in mm VLBI. Moreover, closure phases measure primarily the orientation, shape, and distance between major bright regions in the image, making them optimal to search for time periodicities in the image structure.

Figure 12 shows the effect of a number of example models of orbiting “hot spots” around Sgr A\* on the time evolution of the closure phases along representative triangles of baselines. Simple periodicity searches can easily

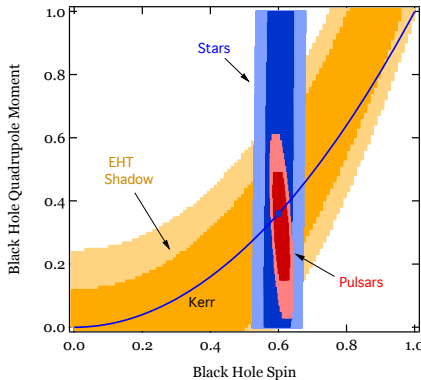


**Fig. 13** Combined constraints on the spin  $a$  and spacetime quadrupole  $q$  of Sgr A\* based on hypothetical measurements of the shape and size of its shadow (orange), of the orbital precession of orbiting stars (blue), and of the timing properties of an orbiting pulsar (red). If the black hole is described by the Kerr metric, the measurements should lie on the thin blue line for which  $q = -a^2$ . Each of these measurements faces different challenges and potential systematic effects. Statistical agreement between the three measurements will increase substantially their credibility [50].

detect quasi periodicities in such signals as well as measure their frequencies and coherence.

If such quasi-periodic signals are detected from Sgr A\* with the EHT, the main challenge of performing gravity tests with them will be in identifying their physical origin, i.e., the oscillatory mode they correspond to. As Figure 10 shows, the detection of a single period between 4–100 min can be attributed to different linear modes or to different values of the black-hole spin. Even the simultaneous detection of three different periods may not lead to a conclusive result unless they are securely identified with particular oscillatory modes or non-linear resonances.

The problem discussed above have severely hampered the ability to perform similar tests of gravity with observations of quasi-periodic oscillations from stellar-mass black holes (see discussion in [144]). In the case of observations with the EHT, the closure phases will provide not only measurements of the characteristic oscillatory periods but also detailed information on the relative sizes, shapes, and orientations of the structures that cause them. Because each oscillatory mode corresponds to a very particular structure in the accretion flow, it is possible that such information will provide enough clues to identify each period with a particular mode and lead to quantitative measurements of the black-hole spin in Sgr A\* and to tests of gravity.

## 7 Combining Tests with the EHT, Stars, and Pulsars

As discussed in the previous sections, the EHT offers more than one ways of testing gravity with its primary targets based on either imaging or timing

observations. In the case of Sgr A\*, there are also additional avenues of testing gravity using stars and pulsars that lie on close elliptical orbits around the black hole [151].

Ref. [152] proposed a test of the no-hair theorem, i.e., an independent measurement of the black-hole spin and quadrupole moment, based on measuring the rate of precession of the periapsis and of the plane of the orbits of stars. A number of studies have since explored the requirements on the stellar orbits for such a measurement and the potential complexities introduced by the presence of other stars and gas in the vicinity of the black hole [153, 154, 155, 156, 157, 158, 50, 159, 160]. There is, indeed, a sweet spot of semi-major axes of  $\sim 300 - 5000GM/c^2$  for the orbits of stars that are optimal for measuring spacetime parameters for Sgr A\*. If such stars are discovered and monitored, they will lead to measurements of the spin of the black hole with an accuracy of  $\sim 10\%$  and a weak constraint on its quadrupole moment (see Fig. 13) [50, 160].

Even though detecting the precession of a stellar orbit requires continuous monitoring over multiple orbital periods and is susceptible to various astrophysical complications, timing of even a single slow pulsar in close orbit during a few periapsis passages will lead to an accurate measurement of the spacetime moments of the black hole [161, 162, 50, 163]. This is true because the time-of-arrival of the pulsar signal depends on the properties of the spacetime along the line of sight from the current location of the pulsar to the distant observer. As the relative position of the pulsar, the black hole, and the spacetime evolve during the periapsis passage, this allows mapping the spacetime and measuring its properties, without requiring to wait for observing actual orbital precession.

Figure 13 shows the combined constraints on the spin  $a$  and the quadrupole moment  $q$  of Sgr A\* based on a hypothetical measurement of the shape and size of its shadow with the EHT, of the orbital precession of orbiting stars, and of the timing properties of an orbiting pulsar. As discussed in the previous sections, the shadow measurement will constrain any possible deviations from the no-hair relation  $q = -a^2$ ; the precession of stellar orbits will measure primarily the black-hole spin; and the timing of a pulsar will measure the black-hole spin and its quadrupole moment. The three types of measurements involve very different observations and techniques and potentially suffer from uncorrelated biases. Moreover, they lead to nearly orthogonal measurements of the spacetime moments. Performing such measurements and generating results that are in statistical agreement with each other will lead to highly credible tests of gravity in the near horizon of an astrophysical, supermassive black hole, with the Event Horizon Telescope.

**Acknowledgements** I thank my colleagues and students at the University of Arizona and especially T. Johannsen, J. Kim, L. Medeiros, C. K. Chan, F. Özel and D. Marrone, who have contributed substantially to most of the work presented in this review. I also thank all the members of the EHT collaboration, who have made this incredible project a reality. Writing of this review has been supported by NSF PIRE grant 1743747.

## References

1. B. Balick, R.L. Brown, *ApJ* **194**, 265 (1974). <https://doi.org/10.1086/153242>
2. R.D. Davies, D. Walsh, R.S. Booth, *MNRAS* **177**, 319 (1976). <https://doi.org/10.1093/mnras/177.2.319>
3. K.Y. Lo, D.C. Backer, R.D. Ekers, K.I. Kellermann, M. Reid, J.M. Moran, *Nature* **315**, 124 (1985). <https://doi.org/10.1038/315124a0>
4. G.C. Bower, H. Falcke, R.M. Herrnstein, J.H. Zhao, W.M. Goss, D.C. Backer, *Science* **304**, 704 (2004). <https://doi.org/10.1126/science.1094023>. [[astro-ph/0404001](#)]
5. G.C. Bower, W.M. Goss, H. Falcke, D.C. Backer, Y. Lithwick, *ApJ* **648**, L127 (2006). <https://doi.org/10.1086/508019>. [[astro-ph/0608004](#)]
6. D.C. Backer, *ApJ* **222**, L9 (1978). <https://doi.org/10.1086/182681>
7. R. Narayan, J. Goodman, *MNRAS* **238**, 963 (1989)
8. J. Goodman, R. Narayan, *MNRAS* **238**, 995 (1989)
9. H.J. van Langevelde, D.A. Frail, J.M. Cordes, P.J. Diamond, *ApJ* **396**, 686 (1992). <https://doi.org/10.1086/171750>
10. T.J.W. Lazio, J.M. Cordes, *ApJ* **505**, 715 (1998). <https://doi.org/10.1086/306174>. [[astro-ph/9804157](#)]
11. T.J.W. Lazio, J.M. Cordes, *ApJS* **118**, 201 (1998). <https://doi.org/10.1086/313129>. [[astro-ph/9804156](#)]
12. K.Y. Lo, D.C. Backer, K.I. Kellermann, M. Reid, J.H. Zhao, W.M. Goss, J.M. Moran, *Nature* **362**, 38 (1993). <https://doi.org/10.1038/362038a0>
13. T.P. Krichbaum, D.A. Graham, A. Witzel, A. Greve, J.E. Wink, M. Grewing, F. Colomer, P. de Vicente, J. Gomez-Gonzalez, A. Baudry, J.A. Zensus, *A&A* **335**, L106 (1998)
14. Z.Q. Shen, K.Y. Lo, M.C. Liang, P.T.P. Ho, J.H. Zhao, *Nature* **438**, 62 (2005). <https://doi.org/10.1038/nature04205>. [[astro-ph/0512515](#)]
15. N.I. Shakura, R.A. Sunyaev, *A&A* **24**, 337 (1973)
16. I.D. Novikov, K.S. Thorne, in *Black Holes (Les Astres Occlus)*, ed. by C. DeWitt, B.S. DeWitt (1973), pp. 343–450
17. R. Narayan, I. Yi, *ApJ* **428**, L13 (1994). <https://doi.org/10.1086/187381>. [[astro-ph/9403052](#)]
18. R. Narayan, I. Yi, *ApJ* **452**, 710 (1995). <https://doi.org/10.1086/176343>. [[astro-ph/9411059](#)]
19. R. Narayan, I. Yi, R. Mahadevan, *Nature* **374**, 623 (1995). <https://doi.org/10.1038/374623a0>
20. T. Di Matteo, E. Quataert, S.W. Allen, R. Narayan, A.C. Fabian, *MNRAS* **311**, 507 (2000). <https://doi.org/10.1046/j.1365-8711.2000.03134.x>. [[astro-ph/9905053](#)]
21. H. Falcke, W.M. Goss, H. Matsuo, P. Teuben, J.H. Zhao, R. Zylka, *ApJ* **499**, 731 (1998). <https://doi.org/10.1086/305687>. [[astro-ph/9801085](#)]
22. F. Özel, D. Psaltis, R. Narayan, *ApJ* **541**, 234 (2000). <https://doi.org/10.1086/309396>. [[astro-ph/0004195](#)]
23. J.M. Bardeen, in *Black Holes (Les Astres Occlus)*, ed. by C. DeWitt, B.S. DeWitt (1973), pp. 215–239
24. J.P. Luminet, *A&A* **75**, 228 (1979)
25. H. Falcke, S. Markoff, *A&A* **362**, 113 (2000). [[astro-ph/0102186](#)]
26. A.E. Broderick, A. Loeb, *ApJ* **636**, L109 (2006). <https://doi.org/10.1086/500008>. [[astro-ph/0508386](#)]
27. T.P. Krichbaum, J.A. Zensus, A. Witzel, P.G. Mezger, K.J. Standke, C.J. Schalinski, A. Alberdi, J.M. Marcaide, R. Zylka, A.E.E. Rogers, R.S. Booth, B.O. Ronnang, F. Colomer, N. Bartel, I.I. Shapiro, *A&A* **274**, L37 (1993)
28. D.C. Backer, J.A. Zensus, K.I. Kellermann, M. Reid, J.M. Moran, K.Y. Lo, *Science* **262**, 1414 (1993). <https://doi.org/10.1126/science.262.5138.1414>
29. A.E.E. Rogers, S. Doeleman, M.C.H. Wright, G.C. Bower, D.C. Backer, S. Padin, J.A. Philips, D.T. Emerson, L. Greenhill, J.M. Moran, K.I. Kellermann, *ApJ* **434**, L59 (1994). <https://doi.org/10.1086/187574>

30. S.S. Doeleman, J. Weintraub, A.E.E. Rogers, R. Plambeck, R. Freund, R.P.J. Tilanus, P. Friberg, L.M. Ziurys, J.M. Moran, B. Corey, K.H. Young, D.L. Smythe, M. Titus, D.P. Marrone, R.J. Cappallo, D.C.J. Bock, G.C. Bower, R. Chamberlin, G.R. Davis, T.P. Krichbaum, J. Lamb, H. Maness, A.E. Niell, A. Roy, P. Strittmatter, D. Werthimer, A.R. Whitney, D. Woody, *Nature* **455**, 78 (2008). <https://doi.org/10.1038/nature07245>. [[arXiv:0809.2442](https://arxiv.org/abs/0809.2442)]
31. S.S. Doeleman, V.L. Fish, D.E. Schenck, C. Beaudoin, R. Blundell, G.C. Bower, A.E. Broderick, R. Chamberlin, R. Freund, P. Friberg, M.A. Gurwell, P.T.P. Ho, M. Honma, M. Inoue, T.P. Krichbaum, J. Lamb, A. Loeb, C. Lonsdale, D.P. Marrone, J.M. Moran, T. Oyama, R. Plambeck, R.A. Primiani, A.E.E. Rogers, D.L. Smythe, J. SooHoo, P. Strittmatter, R.P.J. Tilanus, M. Titus, J. Weintraub, M. Wright, K.H. Young, L.M. Ziurys, *Science* **338**, 355 (2012). <https://doi.org/10.1126/science.1224768>. [[arXiv:1210.6132 \[astro-ph.HE\]](https://arxiv.org/abs/1210.6132)]
32. S. Doeleman, E. Agol, D. Backer, F. Baganoff, G.C. Bower, A. Broderick, A. Fabian, V. Fish, C. Gammie, P. Ho, M. Honma, T. Krichbaum, A. Loeb, D. Marrone, M. Reid, A. Rogers, I. Shapiro, P. Strittmatter, R. Tilanus, J. Weintraub, A. Whitney, M. Wright, L. Ziurys, in *astro2010: The Astronomy and Astrophysics Decadal Survey, Astronomy*, vol. 2010 (2009), *Astronomy*, vol. 2010, p. 68
33. V.L. Fish, K. Akiyama, K.L. Bouman, A.A. Chael, M.D. Johnson, S.S. Doeleman, L. Blackburn, J.F.C. Wardle, W.T. Freeman, the Event Horizon Telescope Collaboration, ArXiv e-prints (2016). [[arXiv:1607.03034 \[astro-ph.IM\]](https://arxiv.org/abs/1607.03034)]
34. M.D. Johnson, collaborators, *Science* (2015)
35. M. Honma, K. Akiyama, M. Uemura, S. Ikeda, *PASJ* **66**, 95 (2014). <https://doi.org/10.1093/pasj/psu070>
36. K.L. Bouman, M.D. Johnson, D. Zoran, V.L. Fish, S.S. Doeleman, W.T. Freeman, in *The IEEE Conference on Computer Vision and Pattern Recognition (CVPR)* (2016)
37. A.A. Chael, M.D. Johnson, R. Narayan, S.S. Doeleman, J.F.C. Wardle, K.L. Bouman, *ApJ* **829**, 11 (2016). <https://doi.org/10.3847/0004-637X/829/1/11>. [[arXiv:1605.06156 \[astro-ph.IM\]](https://arxiv.org/abs/1605.06156)]
38. K. Akiyama, S. Ikeda, M. Pleau, V.L. Fish, F. Tazaki, K. Kuramochi, A.E. Broderick, J. Dexter, M. Mościbrodzka, M. Gowanlock, M. Honma, S.S. Doeleman, *AJ* **153**, 159 (2017). <https://doi.org/10.3847/1538-3881/aa6302>. [[arXiv:1702.00424 \[astro-ph.IM\]](https://arxiv.org/abs/1702.00424)]
39. K.L. Bouman, M.D. Johnson, A.V. Dalca, A.A. Chael, F. Roelofs, S.S. Doeleman, W.T. Freeman, ArXiv e-prints (2017). [[arXiv:1711.01357 \[astro-ph.IM\]](https://arxiv.org/abs/1711.01357)]
40. M.D. Johnson, K.L. Bouman, L. Blackburn, A.A. Chael, J. Rosen, H. Shiokawa, F. Roelofs, K. Akiyama, V.L. Fish, S.S. Doeleman, *ApJ* **850**, 172 (2017). <https://doi.org/10.3847/1538-4357/aa97dd>. [[arXiv:1711.01286 \[astro-ph.IM\]](https://arxiv.org/abs/1711.01286)]
41. A.A. Chael, M.D. Johnson, K.L. Bouman, L.L. Blackburn, K. Akiyama, R. Narayan, ArXiv e-prints (2018). [[arXiv:1803.07088 \[astro-ph.IM\]](https://arxiv.org/abs/1803.07088)]
42. V.L. Fish, M.D. Johnson, R.S. Lu, S.S. Doeleman, K.L. Bouman, D. Zoran, W.T. Freeman, D. Psaltis, R. Narayan, V. Pankratius, A.E. Broderick, C.R. Gwinn, L.E. Vertatschitsch, *ApJ* **795**, 134 (2014). <https://doi.org/10.1088/0004-637X/795/2/134>. [[arXiv:1409.4690 \[astro-ph.IM\]](https://arxiv.org/abs/1409.4690)]
43. M.D. Johnson, C.R. Gwinn, *ApJ* **805**, 180 (2015). <https://doi.org/10.1088/0004-637X/805/2/180>. [[arXiv:1502.05722 \[astro-ph.IM\]](https://arxiv.org/abs/1502.05722)]
44. M.D. Johnson, *ApJ* **833**, 74 (2016). <https://doi.org/10.3847/1538-4357/833/1/74>. [[arXiv:1610.05326 \[astro-ph.IM\]](https://arxiv.org/abs/1610.05326)]
45. M.D. Johnson, R. Narayan, *ApJ* **826**, 170 (2016). <https://doi.org/10.3847/0004-637X/826/2/170>. [[arXiv:1606.06315 \[astro-ph.IM\]](https://arxiv.org/abs/1606.06315)]
46. R. Gold, J.C. McKinney, M.D. Johnson, S.S. Doeleman, *ApJ* **837**, 180 (2017). <https://doi.org/10.3847/1538-4357/aa6193>. [[arXiv:1601.05550 \[astro-ph.HE\]](https://arxiv.org/abs/1601.05550)]
47. T. Johannsen, D. Psaltis, *ApJ* **718**, 446 (2010). <https://doi.org/10.1088/0004-637X/718/1/446>. [[arXiv:1005.1931 \[astro-ph.HE\]](https://arxiv.org/abs/1005.1931)]
48. A.E. Broderick, T. Johannsen, A. Loeb, D. Psaltis, *ApJ* **784**, 7 (2014). <https://doi.org/10.1088/0004-637X/784/1/7>. [[arXiv:1311.5564 \[astro-ph.HE\]](https://arxiv.org/abs/1311.5564)]
49. D. Psaltis, F. Özel, C.K. Chan, D.P. Marrone, *ApJ* **814**, 115 (2015). <https://doi.org/10.1088/0004-637X/814/2/115>. [[arXiv:1411.1454 \[astro-ph.HE\]](https://arxiv.org/abs/1411.1454)]
50. D. Psaltis, N. Wex, M. Kramer, *ApJ* **818**, 121 (2016). <https://doi.org/10.3847/0004-637X/818/2/121>. [[arXiv:1510.00394 \[astro-ph.HE\]](https://arxiv.org/abs/1510.00394)]

51. A.E. Broderick, V.L. Fish, S.S. Doeleman, A. Loeb, *ApJ* **697**, 45 (2009). <https://doi.org/10.1088/0004-637X/697/1/45>. [[arXiv:0809.4490](https://arxiv.org/abs/0809.4490)]
52. A.B. Kamruddin, J. Dexter, *MNRAS* **434**, 765 (2013). <https://doi.org/10.1093/mnras/stt1068>. [[arXiv:1306.3226 \[astro-ph.HE\]](https://arxiv.org/abs/1306.3226)]
53. L. Benkevitch, K. Akiyama, R. Lu, S. Doeleman, V. Fish, ArXiv e-prints (2016). [[arXiv:1609.00055 \[astro-ph.IM\]](https://arxiv.org/abs/1609.00055)]
54. J. Kim, D.P. Marrone, C.K. Chan, L. Medeiros, F. Özel, D. Psaltis, *ApJ* **832**, 156 (2016). <https://doi.org/10.3847/0004-637X/832/2/156>. [[arXiv:1602.00692 \[astro-ph.HE\]](https://arxiv.org/abs/1602.00692)]
55. M. Mościbrodzka, C.F. Gammie, J.C. Dolence, H. Shiokawa, P.K. Leung, *ApJ* **706**, 497 (2009). <https://doi.org/10.1088/0004-637X/706/1/497>. [[arXiv:0909.5431 \[astro-ph.HE\]](https://arxiv.org/abs/0909.5431)]
56. M. Mościbrodzka, H. Falcke, H. Shiokawa, C.F. Gammie, *A&A* **570**, A7 (2014). <https://doi.org/10.1051/0004-6361/201424358>. [[arXiv:1408.4743 \[astro-ph.HE\]](https://arxiv.org/abs/1408.4743)]
57. J. Dexter, E. Agol, P.C. Fragile, *ApJ* **703**, L142 (2009). <https://doi.org/10.1088/0004-637X/703/2/L142>. [[arXiv:0909.0267 \[astro-ph.HE\]](https://arxiv.org/abs/0909.0267)]
58. J. Dexter, E. Agol, P.C. Fragile, J.C. McKinney, *ApJ* **717**, 1092 (2010). <https://doi.org/10.1088/0004-637X/717/2/1092>. [[arXiv:1005.4062 \[astro-ph.HE\]](https://arxiv.org/abs/1005.4062)]
59. C.K. Chan, D. Psaltis, F. Özel, R. Narayan, A. Sadowski, *ApJ* **799**, 1 (2015). <https://doi.org/10.1088/0004-637X/799/1/1>. [[arXiv:1410.3492 \[astro-ph.HE\]](https://arxiv.org/abs/1410.3492)]
60. S.M. Ressler, A. Tchekhovskoy, E. Quataert, M. Chandra, C.F. Gammie, *MNRAS* **454**, 1848 (2015). <https://doi.org/10.1093/mnras/stv2084>. [[arXiv:1509.04717 \[astro-ph.HE\]](https://arxiv.org/abs/1509.04717)]
61. O. Porth, H. Olivares, Y. Mizuno, Z. Younsi, L. Rezzolla, M. Moscibrodzka, H. Falcke, M. Kramer, ArXiv e-prints (2016). [[arXiv:1611.09720 \[gr-qc\]](https://arxiv.org/abs/1611.09720)]
62. S.M. Ressler, A. Tchekhovskoy, E. Quataert, C.F. Gammie, *MNRAS* **467**, 3604 (2017). <https://doi.org/10.1093/mnras/stx364>. [[arXiv:1611.09365 \[astro-ph.HE\]](https://arxiv.org/abs/1611.09365)]
63. L. Medeiros, C.K. Chan, F. Özel, D. Psaltis, J. Kim, D.P. Marrone, A. Sadowski, ArXiv e-prints (2016). [[arXiv:1601.06799 \[astro-ph.HE\]](https://arxiv.org/abs/1601.06799)]
64. L. Medeiros, C.K. Chan, F. Özel, D. Psaltis, J. Kim, D. Marrone, A. Sadowski, ArXiv e-prints (2016). [[arXiv:1610.03505 \[astro-ph.HE\]](https://arxiv.org/abs/1610.03505)]
65. M. Mościbrodzka, H. Falcke, H. Shiokawa, *A&A* **586**, A38 (2016). <https://doi.org/10.1051/0004-6361/201526630>. [[arXiv:1510.07243 \[astro-ph.HE\]](https://arxiv.org/abs/1510.07243)]
66. M. Mościbrodzka, J. Dexter, J. Davelaar, H. Falcke, *MNRAS* **468**, 2214 (2017). <https://doi.org/10.1093/mnras/stx587>. [[arXiv:1703.02390 \[astro-ph.HE\]](https://arxiv.org/abs/1703.02390)]
67. C.M. Will, *Living Reviews in Relativity* **17**, 4 (2014). <https://doi.org/10.12942/lrr-2014-4>. [[arXiv:1403.7377 \[gr-qc\]](https://arxiv.org/abs/1403.7377)]
68. D. Psaltis, *Living Reviews in Relativity* **11**, 9 (2008). <https://doi.org/10.12942/lrr-2008-9>. [[arXiv:0806.1531](https://arxiv.org/abs/0806.1531)]
69. E. Berti, E. Barausse, V. Cardoso, L. Gualtieri, P. Pani, U. Sperhake, L.C. Stein, N. Wex, K. Yagi, T. Baker, C.P. Burgess, F.S. Coelho, D. Doneva, A. De Felice, P.G. Ferreira, P.C.C. Freire, J. Healy, C. Herdeiro, M. Horbatsch, B. Kleihaus, A. Klein, K. Kokkotas, J. Kunz, P. Laguna, R.N. Lang, T.G.F. Li, T. Littenberg, A. Matas, S. Mirshekari, H. Okawa, E. Radu, R. O'Shaughnessy, B.S. Sathyaprakash, C. Van Den Broeck, H.A. Winther, H. Witek, M. Emad Aghili, J. Alsing, B. Bolen, L. Bombelli, S. Caudill, L. Chen, J.C. Degollado, R. Fujita, C. Gao, D. Gerosa, S. Kamali, H.O. Silva, J.G. Rosa, L. Sadeghian, M. Sampaio, H. Sotani, M. Zilhao, *Classical and Quantum Gravity* **32**(24), 243001 (2015). <https://doi.org/10.1088/0264-9381/32/24/243001>. [[arXiv:1501.07274 \[gr-qc\]](https://arxiv.org/abs/1501.07274)]
70. K. Koyama, *Reports on Progress in Physics* **79**(4), 046902 (2016). <https://doi.org/10.1088/0034-4885/79/4/046902>. [[arXiv:1504.04623](https://arxiv.org/abs/1504.04623)]
71. B.P. Abbott, R. Abbott, T.D. Abbott, M.R. Abernathy, F. Acernese, K. Ackley, C. Adams, T. Adams, P. Addesso, R.X. Adhikari, et al., *Physical Review Letters* **116**(22), 221101 (2016). <https://doi.org/10.1103/PhysRevLett.116.221101>. [[arXiv:1602.03841 \[gr-qc\]](https://arxiv.org/abs/1602.03841)]
72. G. 't Hooft, S.B. Giddings, C. Rovelli, P. Nicolini, J. Mureika, M. Kaminski, M. Bleicher, ArXiv e-prints (2016). [[arXiv:1609.01725 \[hep-th\]](https://arxiv.org/abs/1609.01725)]
73. A. Almheiri, D. Marolf, J. Polchinski, J. Sully, *Journal of High Energy Physics* **2**, 62 (2013). [https://doi.org/10.1007/JHEP02\(2013\)062](https://doi.org/10.1007/JHEP02(2013)062). [[arXiv:1207.3123 \[hep-th\]](https://arxiv.org/abs/1207.3123)]

- 
74. S.B. Giddings, Nature Astronomy **1**, 0067 (2017). <https://doi.org/10.1038/s41550-017-0067>. [[arXiv:1703.03387 \[gr-qc\]](#)]
  75. T. Baker, D. Psaltis, C. Skordis, ApJ **802**, 63 (2015). <https://doi.org/10.1088/0004-637X/802/1/63>. [[arXiv:1412.3455](#)]
  76. A. Joyce, B. Jain, J. Khoury, M. Trodden, Phys. Rep. **568**, 1 (2015). <https://doi.org/10.1016/j.physrep.2014.12.002>. [[arXiv:1407.0059](#)]
  77. K. Yagi, L.C. Stein, N. Yunes, Phys. Rev. D **93**(2), 024010 (2016). <https://doi.org/10.1103/PhysRevD.93.024010>. [[arXiv:1510.02152 \[gr-qc\]](#)]
  78. A. Hees, T. Do, A.M. Ghez, G.D. Martinez, S. Naoz, E.E. Becklin, A. Boehle, S. Chappell, D. Chu, A. Dehghanfar, K. Kosmo, J.R. Lu, K. Matthews, M.R. Morris, S. Sakai, R. Schödel, G. Witzel, Physical Review Letters **118**(21), 211101 (2017). <https://doi.org/10.1103/PhysRevLett.118.211101>. [[arXiv:1705.07902](#)]
  79. S.A. Hughes, in *Laser Interferometer Space Antenna: 6th International LISA Symposium, American Institute of Physics Conference Series*, vol. 873, ed. by S.M. Merkowitz, J.C. Livas (2006), *American Institute of Physics Conference Series*, vol. 873, pp. 233–240. <https://doi.org/10.1063/1.2405049>
  80. D. Psaltis, D. Perrodin, K.R. Dienes, I. Mocioiu, Physical Review Letters **100**(9), 091101 (2008). <https://doi.org/10.1103/PhysRevLett.100.091101>
  81. E. Barausse, T.P. Sotiriou, Physical Review Letters **101**(9), 099001 (2008). <https://doi.org/10.1103/PhysRevLett.101.099001>. [[arXiv:0803.3433 \[gr-qc\]](#)]
  82. T.P. Sotiriou, V. Faraoni, Physical Review Letters **108**(8), 081103 (2012). <https://doi.org/10.1103/PhysRevLett.108.081103>. [[arXiv:1109.6324 \[gr-qc\]](#)]
  83. E. Berti, A. Sesana, E. Barausse, V. Cardoso, K. Belczynski, Physical Review Letters **117**(10), 101102 (2016). <https://doi.org/10.1103/PhysRevLett.117.101102>. [[arXiv:1605.09286 \[gr-qc\]](#)]
  84. T. Johannsen, D. Psaltis, ApJ **716**, 187 (2010). <https://doi.org/10.1088/0004-637X/716/1/187>. [[arXiv:1003.3415 \[astro-ph.HE\]](#)]
  85. E. Teo, General Relativity and Gravitation **35**, 1909 (2003). <https://doi.org/10.1023/A:1026286607562>
  86. P.V.P. Cunha, C.A.R. Herdeiro, E. Radu, Phys. Rev. D **96**(2), 024039 (2017). <https://doi.org/10.1103/PhysRevD.96.024039>. [[arXiv:1705.05461 \[gr-qc\]](#)]
  87. J.M. Bardeen, W.H. Press, S.A. Teukolsky, ApJ **178**, 347 (1972). <https://doi.org/10.1086/151796>
  88. S. Chandrasekhar, *The mathematical theory of black holes* (1983)
  89. R. Takahashi, ApJ **611**, 996 (2004). <https://doi.org/10.1086/422403>. [[astro-ph/0405099](#)]
  90. V. Bozza, F. de Luca, G. Scarpetta, Phys. Rev. D **74**(6), 063001 (2006). <https://doi.org/10.1103/PhysRevD.74.063001>. [[gr-qc/0604093](#)]
  91. C.k. Chan, D. Psaltis, F. Özel, ApJ **777**, 13 (2013). <https://doi.org/10.1088/0004-637X/777/1/13>. [[arXiv:1303.5057 \[astro-ph.IM\]](#)]
  92. T. Johannsen, ApJ **777**, 170 (2013). <https://doi.org/10.1088/0004-637X/777/2/170>. [[arXiv:1501.02814 \[astro-ph.HE\]](#)]
  93. C. Bambi, K. Freese, Phys. Rev. D **79**(4), 043002 (2009). <https://doi.org/10.1103/PhysRevD.79.043002>. [[arXiv:0812.1328](#)]
  94. R. Shaikh, P. Kocherlakota, R. Narayan, P.S. Joshi, ArXiv e-prints (2018). [[arXiv:1802.08060 \[astro-ph.HE\]](#)]
  95. S.B. Giddings, D. Psaltis, ArXiv e-prints (2016). [[arXiv:1606.07814 \[astro-ph.HE\]](#)]
  96. D. Psaltis, R. Narayan, V.L. Fish, A.E. Broderick, A. Loeb, S.S. Doeleman, ApJ **798**, 15 (2015). <https://doi.org/10.1088/0004-637X/798/1/15>. [[arXiv:1409.5447 \[astro-ph.HE\]](#)]
  97. A. Boehle, A.M. Ghez, R. Schödel, L. Meyer, S. Yelda, S. Albers, G.D. Martinez, E.E. Becklin, T. Do, J.R. Lu, K. Matthews, M.R. Morris, B. Sitarski, G. Witzel, ApJ **830**, 17 (2016). <https://doi.org/10.3847/0004-637X/830/1/17>. [[arXiv:1607.05726](#)]
  98. A. de Vries, Classical and Quantum Gravity **17**, 123 (2000). <https://doi.org/10.1088/0264-9381/17/1/309>
  99. R. Takahashi, PASJ **57**, 273 (2005). <https://doi.org/10.1093/pasj/57.2.273>. [[astro-ph/0505316](#)]
  100. C. Bambi, N. Yoshida, Classical and Quantum Gravity **27**(20), 205006 (2010). <https://doi.org/10.1088/0264-9381/27/20/205006>. [[arXiv:1004.3149 \[gr-qc\]](#)]

101. L. Amarilla, E.F. Eiroa, Phys. Rev. D **85**(6), 064019 (2012). <https://doi.org/10.1103/PhysRevD.85.064019>. [[arXiv:1112.6349 \[gr-qc\]](https://arxiv.org/abs/1112.6349)]
102. A. Abdujabbarov, F. Atamurotov, Y. Kucukakca, B. Ahmedov, U. Camci, Astr. & Space Science **344**, 429 (2013). <https://doi.org/10.1007/s10509-012-1337-6>. [[arXiv:1212.4949 \[physics.gen-ph\]](https://arxiv.org/abs/1212.4949)]
103. F. Atamurotov, A. Abdujabbarov, B. Ahmedov, Astr. & Space Science **348**, 179 (2013). <https://doi.org/10.1007/s10509-013-1548-5>
104. T. Johannsen, ApJ **777**, 170 (2013). <https://doi.org/10.1088/0004-637X/777/2/170>. [[arXiv:1501.02814 \[astro-ph.HE\]](https://arxiv.org/abs/1501.02814)]
105. S.W. Wei, Y.X. Liu, JCAP **11**, 063 (2013). <https://doi.org/10.1088/1475-7516/2013/11/063>. [[arXiv:1311.4251 \[gr-qc\]](https://arxiv.org/abs/1311.4251)]
106. V.K. Tinchev, S.S. Yazadjiev, International Journal of Modern Physics D **23**, 1450060 (2014). <https://doi.org/10.1142/S0218271814500606>. [[arXiv:1311.1353 \[gr-qc\]](https://arxiv.org/abs/1311.1353)]
107. A. Grenzebach, V. Perlick, C. Lämmerzahl, Phys. Rev. D **89**(12), 124004 (2014). <https://doi.org/10.1103/PhysRevD.89.124004>. [[arXiv:1403.5234 \[gr-qc\]](https://arxiv.org/abs/1403.5234)]
108. N. Sakai, H. Saida, T. Tamaki, Phys. Rev. D **90**(10), 104013 (2014). <https://doi.org/10.1103/PhysRevD.90.104013>. [[arXiv:1408.6929 \[gr-qc\]](https://arxiv.org/abs/1408.6929)]
109. C. Bambi, Classical and Quantum Gravity **32**(6), 065005 (2015). <https://doi.org/10.1088/0264-9381/32/6/065005>. [[arXiv:1409.0310 \[gr-qc\]](https://arxiv.org/abs/1409.0310)]
110. T. Ohgami, N. Sakai, Phys. Rev. D **91**(12), 124020 (2015). <https://doi.org/10.1103/PhysRevD.91.124020>. [[arXiv:1704.07065 \[gr-qc\]](https://arxiv.org/abs/1704.07065)]
111. S.W. Wei, P. Cheng, Y. Zhong, X.N. Zhou, JCAP **8**, 004 (2015). <https://doi.org/10.1088/1475-7516/2015/08/004>. [[arXiv:1501.06298 \[gr-qc\]](https://arxiv.org/abs/1501.06298)]
112. N. Ortiz, O. Sarbach, T. Zannias, Phys. Rev. D **92**(4), 044035 (2015). <https://doi.org/10.1103/PhysRevD.92.044035>. [[arXiv:1505.07017 \[gr-qc\]](https://arxiv.org/abs/1505.07017)]
113. P.V.P. Cunha, C.A.R. Herdeiro, E. Radu, H.F. Rúnarsson, International Journal of Modern Physics D **25**, 1641021 (2016). <https://doi.org/10.1142/S0218271816410212>. [[arXiv:1605.08293 \[gr-qc\]](https://arxiv.org/abs/1605.08293)]
114. Z. Younsi, A. Zhidenko, L. Rezzolla, R. Konoplya, Y. Mizuno, Phys. Rev. D **94**(8), 084025 (2016). <https://doi.org/10.1103/PhysRevD.94.084025>. [[arXiv:1607.05767 \[gr-qc\]](https://arxiv.org/abs/1607.05767)]
115. F.H. Vincent, E. Gourgoulhon, C. Herdeiro, E. Radu, Phys. Rev. D **94**(8), 084045 (2016). <https://doi.org/10.1103/PhysRevD.94.084045>. [[arXiv:1606.04246 \[gr-qc\]](https://arxiv.org/abs/1606.04246)]
116. A. Alhamzawi, International Journal of Modern Physics D **26**, 1750156-2435 (2017). <https://doi.org/10.1142/S0218271817501565>
117. M. Cvetic, G.W. Gibbons, C.N. Pope, JCAP **8**, 016 (2017). <https://doi.org/10.1088/1475-7516/2017/08/016>. [[arXiv:1705.05740 \[gr-qc\]](https://arxiv.org/abs/1705.05740)]
118. M. Wang, S. Chen, J. Jing, JCAP **10**, 051 (2017). <https://doi.org/10.1088/1475-7516/2017/10/051>. [[arXiv:1707.09451 \[gr-qc\]](https://arxiv.org/abs/1707.09451)]
119. J. Fukue, PASJ **55**, 155 (2003). <https://doi.org/10.1093/pasj/55.1.155>
120. M. Mościbrodzka, H. Shiokawa, C.F. Gammie, J.C. Dolence, ApJ **752**, L1 (2012). <https://doi.org/10.1088/2041-8205/752/1/L1>. [[arXiv:1204.1371 \[astro-ph.HE\]](https://arxiv.org/abs/1204.1371)]
121. H.Y. Pu, K. Akiyama, K. Asada, ApJ **831**, 4 (2016). <https://doi.org/10.3847/0004-637X/831/1/4>. [[arXiv:1608.03035 \[astro-ph.HE\]](https://arxiv.org/abs/1608.03035)]
122. T. Johannsen, A.E. Broderick, P.M. Plewa, S. Chatzopoulos, S.S. Doeleman, F. Eisenhauer, V.L. Fish, R. Genzel, O. Gerhard, M.D. Johnson, Physical Review Letters **116**(3), 031101 (2016). <https://doi.org/10.1103/PhysRevLett.116.031101>. [[arXiv:1512.02640](https://arxiv.org/abs/1512.02640)]
123. R.A. Remillard, J.E. McClintock, ARA&A **44**, 49 (2006). <https://doi.org/10.1146/annurev.astro.44.051905.092532>. [[astro-ph/0606352](https://arxiv.org/abs/0606352)]
124. R. Genzel, R. Schödel, T. Ott, A. Eckart, T. Alexander, F. Lacombe, D. Rouan, B. Aschenbach, Nature **425**, 934 (2003). <https://doi.org/10.1038/nature02065>. [[astro-ph/0310821](https://arxiv.org/abs/0310821)]
125. T. Do, A.M. Ghez, M.R. Morris, S. Yelda, L. Meyer, J.R. Lu, S.D. Hornstein, K. Matthews, ApJ **691**, 1021 (2009). <https://doi.org/10.1088/0004-637X/691/2/1021>. [[arXiv:0810.0446](https://arxiv.org/abs/0810.0446)]
126. J. Neilsen, M.A. Nowak, C. Gammie, J. Dexter, S. Markoff, D. Haggard, S. Nayakshin, Q.D. Wang, N. Gross, D. Porquet, J.A. Tomsick, N. Degenaar, P.C. Fragile, J.C. Houck, R. Wijnands, J.M. Miller, F.K. Baganoff, ApJ **774**, 42 (2013). <https://doi.org/10.1088/0004-637X/774/1/42>. [[arXiv:1307.5843 \[astro-ph.HE\]](https://arxiv.org/abs/1307.5843)]

127. K.P. Rauch, R.D. Blandford, ApJ **421**, 46 (1994). <https://doi.org/10.1086/173625>
128. C.k. Chan, D. Psaltis, F. Özel, L. Medeiros, D. Marrone, A. Sadowski, R. Narayan, ApJ **812**, 103 (2015). <https://doi.org/10.1088/0004-637X/812/2/103>. [arXiv:1505.01500 [astro-ph.HE]]
129. L. Meyer, T. Do, A. Ghez, M.R. Morris, S. Yelda, R. Schödel, A. Eckart, ApJ **694**, L87 (2009). <https://doi.org/10.1088/0004-637X/694/1/L87>. [arXiv:0902.2475 [astro-ph.GA]]
130. J. Dexter, B. Kelly, G.C. Bower, D.P. Marrone, J. Stone, R. Plambeck, MNRAS **442**, 2797 (2014). <https://doi.org/10.1093/mnras/stu1039>. [arXiv:1308.5968 [astro-ph.HE]]
131. G.C. Bower, J. Dexter, S. Markoff, M.A. Gurwell, R. Rao, I. McHardy, ApJ **811**, L6 (2015). <https://doi.org/10.1088/2041-8205/811/1/L6>. [arXiv:1508.06603 [astro-ph.HE]]
132. D. Psaltis, T. Belloni, M. van der Klis, ApJ **520**, 262 (1999). <https://doi.org/10.1086/307436>. [astro-ph/9902130]
133. R.V. Wagoner, Phys. Rep. **311**, 259 (1999). [https://doi.org/10.1016/S0370-1573\(98\)00104-5](https://doi.org/10.1016/S0370-1573(98)00104-5). [astro-ph/9805028]
134. S. Kato, PASJ **53**, 1 (2001). <https://doi.org/10.1093/pasj/53.1.1>
135. M.A. Abramowicz, V. Karas, W. Kluźniak, W.H. Lee, P. Rebusco, PASJ **55**, 467 (2003). <https://doi.org/10.1093/pasj/55.2.467>. [astro-ph/0302183]
136. W. Kluzioniak, P. Michelson, R.V. Wagoner, ApJ **358**, 538 (1990). <https://doi.org/10.1086/169006>
137. R. Sunyaev, M. Revnivtsev, A&A **358**, 617 (2000). [astro-ph/0003308]
138. A.T. Okazaki, S. Kato, J. Fukue, PASJ **39**, 457 (1987)
139. C.A. Perez, A.S. Silbergleit, R.V. Wagoner, D.E. Lehr, ApJ **476**, 589 (1997). <https://doi.org/10.1086/303658>. [astro-ph/9601146]
140. S. Kato, PASJ **42**, 99 (1990)
141. A.S. Silbergleit, R.V. Wagoner, M. Ortega-Rodríguez, ApJ **548**, 335 (2001). <https://doi.org/10.1086/318659>. [astro-ph/0004114]
142. R.V. Wagoner, A.S. Silbergleit, M. Ortega-Rodríguez, ApJ **559**, L25 (2001). <https://doi.org/10.1086/323655>. [astro-ph/0107168]
143. M.A. Abramowicz, W. Kluźniak, A&A **374**, L19 (2001). <https://doi.org/10.1051/0004-6361:20010791>. [astro-ph/0105077]
144. D. Psaltis, in *X-ray Timing 2003: Rossi and Beyond*, American Institute of Physics Conference Series, vol. 714, ed. by P. Kaaret, F.K. Lamb, J.H. Swank (2004), American Institute of Physics Conference Series, vol. 714, pp. 29–35. <https://doi.org/10.1063/1.1780994>
145. S.E. Motta, T.M. Belloni, L. Stella, T. Muñoz-Darias, R. Fender, MNRAS **437**, 2554 (2014). <https://doi.org/10.1093/mnras/stt2068>. [arXiv:1309.3652 [astro-ph.HE]]
146. S.E. Motta, T. Muñoz-Darias, A. Sanna, R. Fender, T. Belloni, L. Stella, MNRAS **439**, L65 (2014). <https://doi.org/10.1093/mnrasl/sl181>. [arXiv:1312.3114 [astro-ph.HE]]
147. T. Johannsen, D. Psaltis, ApJ **726**, 11 (2011). <https://doi.org/10.1088/0004-637X/726/1/11>. [arXiv:1010.1000 [astro-ph.HE]]
148. C. Bambi, JCAP **9**, 014 (2012). <https://doi.org/10.1088/1475-7516/2012/09/014>. [arXiv:1205.6348 [gr-qc]]
149. S.S. Doeleman, V.L. Fish, A.E. Broderick, A. Loeb, A.E.E. Rogers, ApJ **695**, 59 (2009). <https://doi.org/10.1088/0004-637X/695/1/59>. [arXiv:0809.3424]
150. R. Fraga-Encinas, M. Mościbrodzka, C. Brinkerink, H. Falcke, A&A **588**, A57 (2016). <https://doi.org/10.1051/0004-6361/201527599>. [arXiv:1602.01669]
151. D. Psaltis, T. Johannsen, Journal of Physics Conference Series **283**(1), 012030 (2011). <https://doi.org/10.1088/1742-6596/283/1/012030>. [arXiv:1012.1602 [astro-ph.HE]]
152. C.M. Will, ApJ **674**, L25 (2008). <https://doi.org/10.1086/528847>. [arXiv:0711.1677]
153. D. Merritt, T. Alexander, S. Mikkola, C.M. Will, Phys. Rev. D **81**(6), 062002 (2010). <https://doi.org/10.1103/PhysRevD.81.062002>. [arXiv:0911.4718 [astro-ph.GA]]
154. R. Angélin, P. Saha, D. Merritt, ApJ **720**, 1303 (2010). <https://doi.org/10.1088/0004-637X/720/2/1303>. [arXiv:1007.0007]
155. L. Sadeghian, C.M. Will, Classical and Quantum Gravity **28**(22), 225029 (2011). <https://doi.org/10.1088/0264-9381/28/22/225029>. [arXiv:1106.5056 [gr-qc]]
156. D. Psaltis, ApJ **759**, 130 (2012). <https://doi.org/10.1088/0004-637X/759/2/130>. [arXiv:1112.0026 [astro-ph.HE]]

157. D. Psaltis, G. Li, A. Loeb, ApJ **777**, 57 (2013). <https://doi.org/10.1088/0004-637X/777/1/57>. [[arXiv:1212.3342 \[astro-ph.HE\]](https://arxiv.org/abs/1212.3342)]
158. F. Zhang, Y. Lu, Q. Yu, ApJ **809**, 127 (2015). <https://doi.org/10.1088/0004-637X/809/2/127>. [[arXiv:1508.06293 \[astro-ph.HE\]](https://arxiv.org/abs/1508.06293)]
159. Q. Yu, F. Zhang, Y. Lu, ApJ **827**, 114 (2016). <https://doi.org/10.3847/0004-637X/827/2/114>. [[arXiv:1606.07725 \[astro-ph.HE\]](https://arxiv.org/abs/1606.07725)]
160. I. Waisberg, J. Dexter, S. Gillessen, O. Pfuhl, F. Eisenhauer, P.M. Plewa, M. Bauböck, A. Jimenez-Rosales, M. Habibi, T. Ott, S. von Fellenberg, F. Gao, F. Widmann, R. Genzel, MNRAS **476**, 3600 (2018). <https://doi.org/10.1093/mnras/sty476>. [[arXiv:1802.08198](https://arxiv.org/abs/1802.08198)]
161. K. Liu, N. Wex, M. Kramer, J.M. Cordes, T.J.W. Lazio, ApJ **747**, 1 (2012). <https://doi.org/10.1088/0004-637X/747/1/1>. [[arXiv:1112.2151 \[astro-ph.HE\]](https://arxiv.org/abs/1112.2151)]
162. R. Angélib, P. Saha, MNRAS **444**, 3780 (2014). <https://doi.org/10.1093/mnras/stu1686>. [[arXiv:1408.0283](https://arxiv.org/abs/1408.0283)]
163. F. Zhang, P. Saha, ApJ **849**, 33 (2017). <https://doi.org/10.3847/1538-4357/aa8f47>. [[arXiv:1709.08341](https://arxiv.org/abs/1709.08341)]